AGU ADVANCING EARTH AND SPACE SCIENCES

Water Resources Research

RESEARCH ARTICLE
10.1029/2023WR036155

Mapping Irrigation Methods in the Northwestern US Using Deep Learning Classification

S. K. Nouwakpo[1], D. Bjorneberg[1], K. McGwire[2], and O. Hoque[3]

[1]United States Department of Agriculture, Agricultural Research Service, Kimberly, ID, USA, [2]Division of Earth and Ecosystem Sciences, Desert Research Institute, Reno, NV, USA, [3]Department of Computer Science, University of Virginia, Charlottesville, VA, USA

Key Points:

- A deep learning model was developed to predict the type of irrigation (Flood, Sprinkler or Other) used in areas of the northwestern USA
- Overall the model predicted the right type of irrigation with an accuracy of 78%
- This tool has application in other irrigated agricultural areas of the semi-arid northwest where irrigation methods are varied

Correspondence to:

S. K. Nouwakpo,
kossi.nouwakpo@usda.gov

Citation:

Nouwakpo, S. K., Bjorneberg, D., McGwire, K., & Hoque, O. (2024). Mapping irrigation methods in the northwestern US using deep learning classification. *Water Resources Research*, *60*, e2023WR036155. https://doi.org/10.1029/2023WR036155

Received 28 AUG 2023
Accepted 23 JUL 2024

Author Contributions:

Conceptualization: S. K. Nouwakpo, D. Bjorneberg
Data curation: O. Hoque
Formal analysis: S. K. Nouwakpo
Methodology: K. McGwire
Resources: D. Bjorneberg
Software: S. K. Nouwakpo, O. Hoque
Writing – original draft: S. K. Nouwakpo, D. Bjorneberg
Writing – review & editing: S. K. Nouwakpo, D. Bjorneberg, O. Hoque

Abstract Many agricultural areas of the western United States and other parts of the world practice irrigation using a variety of irrigation methods. Maps of irrigation methods are needed but existing technologies are often unable to distinguish between different irrigation methods when they co-exist on the same landscape. In this study, we develop a deep learning irrigation methods mapping tool for broad scale application. The technique uses a U-Net model trained on Landsat 5- and 8-derived input images. Training data consisted in irrigation method classified as Flood, Sprinkler or Other on agricultural fields from the Utah Water Related Land Use data set and additional labeling in selected areas of southern Idaho. An ensemble of 10 trained models had an overall accuracy of 0.78. Precision for Flood, Sprinkler and Other were 0.73, 0.82, and 0.80 while recall values were 0.75, 0.74, and 0.84 respectively. Model performance was generally stable throughout the training years but varied by areas. The best performance was obtained in regions with uniform irrigation method across large patches while small fields of contrasting irrigation method with their surroundings were inadequately predicted. Model prediction in an irrigated watershed of southern Idaho for 2006, 2011, 2013, and 2016 were consistent with previously published survey data. This methodology provides a tool for water resource managers to estimate irrigation methods in agricultural watersheds where natural precipitation is low during the growing season and irrigation methods include center pivots, wheel lines and flood irrigation.

Plain Language Summary Many agricultural areas of the western United States practice irrigation using a variety of irrigation methods. Irrigation methods can be classified into 3 main groups: surface (or flood), sprinkler systems and micro-irrigation systems. Flood and sprinkler irrigation account for 90% of irrigated areas in the United States but impact water resources differently. Flood irrigation has been associated with many adverse effects on water quality whereas sprinkler systems are promoted as improved irrigation alternatives to preserve water quantity and quality. Maps of irrigation methods are needed to improve assessment of irrigation methods on water quantity and quality. In this study, we develop an irrigation methods mapping tool by training a deep learning model on publicly available satellite imagery. The model was trained on the Utah Water Related Land Use data set and additional data from southern Idaho. The trained model correctly predicted irrigation method over 78% of the test area. This methodology provides a tool for water resource managers to estimate irrigation methods in agricultural watersheds where natural precipitation is low during the growing season and irrigation methods include center pivots, wheel lines and flood irrigation.

1. Introduction

Global demand for freshwater has increased 6-fold over the past 100 years (Wada et al., 2016) and continues to increase at a rate of 1% per year (Food and Agriculture Organization of the United Nations (FAO), 2018). Population growth, economic development and changing consumption patterns are expected to further expand future demand for freshwater (UNESCO, 2018). In the United States, irrigation withdraws the largest share of freshwater resources (118 of 281 billion gallons per day) in 2015 (Dieter et al., 2018). Irrigation increases both quantity and quality of agricultural production but can adversely impact water availability. One of the main factors influencing water availability in irrigated areas is the method of on-farm irrigation used. Irrigation methods can be classified into three broad categories: surface irrigation, sprinkler irrigation and drip irrigation (Brouwer et al., 1988). Surface irrigation involves the delivery of water to the plant by gravity. Common surface irrigation methods include flood or basin irrigation whereby water is allowed to pond over the irrigated field and furrow irrigation in which water is conveyed through regularly spaced small channels prepared in the field. With sprinkler irrigation, water is pumped through pipes and sprayed to the field via nozzles under high pressure while

drip irrigation or micro-irrigation involves the application of water to individual plants with nozzles under low pressure. Of the three categories of irrigation methods, surface and sprinkler irrigation are the most common, making up 90% of irrigation area in the U.S. (USDA-NASS, 2019).

Many studies have compared surface and sprinkler irrigation with respect to their impacts on soil, air, and water resources as well as crop performance. Results from most of these studies demonstrate the superiority of sprinkler systems over surface irrigation due to better control of water distribution. A study of root distribution by Lv et al. (2010) under different irrigation systems revealed a shallower rooting depth under sprinkler irrigation compared to border irrigation (a form of surface irrigation), suggestive of water deficit conditions under the latter irrigation method. Compared to furrow irrigation, sprinkler irrigation was also found beneficial for visual quality of potato tubers (Trout et al., 1994) owing to reduced water stress, improved nitrogen management and evaporative cooling under sprinkler irrigation. Ippolito et al. (2019) reported alterations in soil phosphorus (P) dynamics with furrow irrigation as reduced conditions occurring on frequently flooded fields produced greater inorganic P and plant-extractable P compared to sprinkler-irrigated fields. Biogeochemical processes enabled by transient water logging conditions under flood irrigation were found to enhance emission of nitrous oxide (N_2O) when compared to sprinkler irrigation (Franco-Luesma et al., 2020). Farahani et al. (2020) documented reductions as high as 37% for nitrates and 42% for dissolved P in subsurface drainage water under sprinkler irrigation compared to flood and furrow irrigation. More evidence of increased leaching under flood irrigation compared to sprinkler irrigation was provided by other solute transport tracing methods (Nachabe et al., 1999) and modeling approaches (Naghedifar et al., 2018). Some benefits of flood irrigation over sprinkler irrigation on sugarbeet quality has been reported by Eckhoff and Bergman (2001) but at the expense of increased nitrate leaching to groundwater.

In the western U.S and other dry regions of the world, a variety of irrigation methods co-exist on the landscape. In an irrigated watershed of southern Idaho, Bjorneberg et al. (2020) found that the proportion of the agricultural land irrigated with sprinklers increased from 46% in 2006 to 59% in 2016 as furrow irrigated fields are converted to sprinkler systems. Evaluating the effect of different irrigation methods on basin-scale processes requires accurate information on the location and distribution of the types of irrigation used on-farm across the irrigated landscape. Currently available irrigation mapping products (Pervez & Brown, 2010; Salmon et al., 2015; Siebert et al., 2005, 2015; Xie et al., 2021) distinguish between irrigated and non-irrigated areas at various spatial scales without explicit information on the methods of irrigation. Regional-scale irrigation mapping from remotely sensed data has been the object of many studies. Methodologies developed in some studies (Bazzi et al., 2019; Boken et al., 2004; Thenkabail et al., 2005) aim to identify irrigated fields in regions where both irrigation and rain-fed agriculture co-exist. Efforts have been made to identify center pivot irrigation systems using computer vision and deep learning techniques (de Albuquerque et al., 2020; Rodrigues et al., 2020; Saraiva et al., 2020; Tang et al., 2021; C. X. Zhang et al., 2018). These techniques take advantage of the circular patterns often associated with center pivot irrigation systems and are sufficient in regions where only this irrigation method is used on agricultural fields. Nevertheless, few techniques currently exist to distinguish between various irrigation methods and accurately map irrigation methods in regions where multiple irrigation types co-exist on the landscape. Raei et al. (2022) developed a deep learning approach based on the U-Net architecture to segment multiple irrigation method classes including many sprinkler types, surface irrigation, urban areas and background areas from high-resolution (1-m) aerial images. The proposed approach represents an advance towards an irrigation methods mapping tool but its development and evaluation was limited in geographic scope (2 counties in southern Idaho) and relied on input images that may not be widely available in space and time. In the U.S. for example, the U.S. Geological Survey provides estimates of the spatial extent and water withdrawals associated with different irrigation methods but this information comes from survey data (Painter et al., 2021). An irrigation methods mapping approach that is accurate and responsive to yearly changes in irrigation methods is needed.

Advances in deep learning have enabled the development of a new generation of irrigation mapping and classification tools using remotely sensed spatial data. Convolutional neural networks (CNNs) are a form of deep learning method originally developed in the field of computer vision for image segmentation and classification (Chauhan et al., 2018; Fukushima, 1979). In recent years, CNNs have been growing in popularity for spatial data analysis (Hoeser & Kuenzer, 2020; Huang et al., 2018) owing to their ability to reveal more complex and hierarchical relationships and thus yield better results compared to shallow neural networks and traditional classification approaches (Kattenborn et al., 2021). In the context of irrigation mapping, Saraiva et al. (2020) used a U-Net network architecture, a type of fully convolutional neural network (FCNN), to classify center pivot irrigation with a precision of 99% and a recall (fraction of all center pivots correctly identified as such) of 88% in

Brazil. Using a similar network architecture, Colligan et al. (2022) mapped irrigated areas in the US state of Montana with an overall accuracy of 99% and a precision of 0.85. Raei et al. (2022) achieved performance metrics ranging from 70% to 86% on test data with their proposed U-Net approach to classify irrigation methods. The objective of this study was to develop the first approach to identify and classify irrigation methods in an area where sprinkler and surface irrigation methods co-exist. We propose a deep learning approach using a U-Net architecture taking as input publicly available remote sensing data. The proposed model was trained using the Water Related Land Use (WRLU) data set from the state of Utah (https://gis.utah.gov/data/planning/water-related-land/). The ability of the trained model to identify irrigation methods within and outside of Utah was also evaluated.

2. Materials and Methods

2.1. Study Area and Common Irrigation Methods

This study utilizes the Utah WRLU data set to develop and train the deep learning model for irrigation methods mapping. Utah covers an area of 219,807 Km^2 and spans longitudes 109°W to 114°W and latitudes 37°N to 42°N (Figure 1). Elevation in the state ranges from 664 m at Beaver Dam wash in the southeast to 4,123 m at the summit of King's Peak in the Uinta mountains. Farming accounts for 43,301 Km^2 of the land in the state. Major agricultural products in the state include hay, alfalfa, small grains, corn, livestock, and dairy products (USDA-NASS, 2021). Overall 18% of the agricultural land is irrigated in Utah compared to 25% nationwide (USDA-NASS, 2019). Irrigation is more common on moderately sized farms (20–202 ha) in Utah compared to the national average (25% in Utah vs. 13% nationwide) (USDA-NASS, 2019).

The irrigation methods mapping technique developed in this study was tested outside of the state of Utah in an irrigated region in southern Idaho (Figure 1b). The bounding box of the region spans 114.96°W, 42.40°N on the southwest corner to 114.02°W, 42.66°N to the northeast. This test region is within the Upper Snake Rock (USR) watershed (Hydrologic Unit Code 17040212), a 6,300 km^2 watershed in south-central Idaho with the Snake River as its major river. Annual precipitation in the region is 250 mm and multiple irrigation projects supply as much as five times the natural annual precipitation to support a thriving agricultural industry. Irrigation water for most of the agricultural land within the test region is supplied by the Twin Falls Canal Company (TFCC) irrigation project. TFCC will therefore be used in this paper to refer to the Idaho test region. Land use within the USR watershed is 37% irrigated agriculture, <1% dryland agriculture, and 60% rangeland and forest land with the remainder urban. Overall, 46% of the agricultural land is irrigated in the state of Idaho with nearly 80% of the land on farms greater than 809 ha in size receiving irrigation water. Irrigation methods used on farms in TFCC are similar to those encountered in the state of Utah.

2.2. Description of the Training Data Set Utah Water Related Land Use Data

The Utah WRLU data set was used to train and validate the proposed model. The WRLU data set has been collected and maintained by the Utah Division of Water Resources since 1967 to help develop a State Water Plan. The data set includes information on the types and extent of irrigated crops, the irrigation method as well as information concerning dry agriculture, wetlands, open water, and urban areas (Utah-DNR, 2022). WRLU data for years 2003–2021 were used for this study but no digitized WRLU data was available for 2016 so this year was not used in the training or evaluation. For each year, the WRLU data set consisted in a shapefile of field boundaries with information on crop, irrigation and other land use attributes. For this study, field boundaries associated with agricultural areas were selected (Figure 1c). Irrigation methods for these fields were classified in the data set as flood, sprinkler, drip, dry crop or sub-irrigated. Sprinkler systems can be divided into two broad categories: (a) periodic-move and fixed systems in which the sprinklers remain at a fixed position and (b) continuous move systems in which the sprinklers are automatically moved in a circular or straight path (USDA-NRCS, 2016). The most common sprinkler systems in the region are wheel lines which are periodic-move systems and center pivots which are continuous move systems recognized by their distinctive circular irrigation footprint. Flood irrigation in this data set is synonymous with surface irrigation and encompasses furrow irrigation, basin irrigation, border irrigation and wild flooding (USDA-NRCS, 2012). Furrow and basin irrigation are the most common types of surface irrigation in this region. In basin irrigation, fields are leveled and bordered with dikes to control or prevent runoff while furrow irrigation involves the creation of small channels between crop rows to carry water down the field. Furrow irrigated fields are rarely diked so runoff typically occurs on these

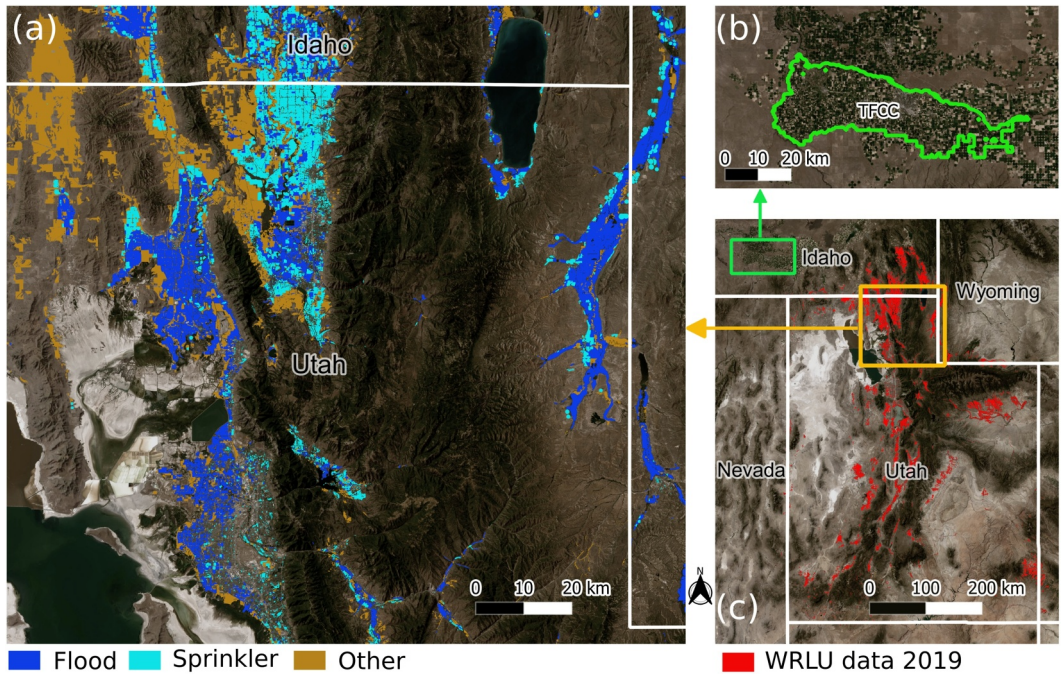

Figure 1. Map of the study area illustrating (a) agricultural fields categorized as Flood, Sprinkler and Other irrigation in a closeup of the 2019 Water Related Land Use (WRLU) for 2019, (b) the Twin Falls Canal Company irrigation project in southern Idaho, and (c) the extent of the WRLU data set. The class Other encompassed non-irrigated areas as well as areas irrigated with less common irrigation methods such as drip irrigation.

fields. The dry crop category correspond to fields without irrigation relying on natural precipitation processes while sub-irrigated fields refer to fields often in riparian areas without irrigation system but receiving additional water due to high water table (Utah Division of Water Resources 2022). In this study, irrigation methods were re-labeled as Flood (F), Sprinkler (S) or Other (O) (Figure 1a). The class O encompassed non-irrigated areas as well as areas irrigated with less common irrigation methods such as drip irrigation.

The WRLU data set was supplemented by additional labeling data collected in and around the TFCC irrigation project. Labeling in the TFCC area was performed within 235 square polygons of size 1.9 Km in which all agricultural fields were labeled with their corresponding irrigation methods. Irrigation identification was performed by a user with knowledge of irrigation methods in the region. Sprinkler- and furrow-irrigated fields were correctly identified by examining field appearances and spatial patterns associated with each irrigation method on high resolution (1 m) aerial imagery from the National Agriculture Imagery Program (NAIP). Field irrigation labels were later reclassified as F, S, or O. Labeling was performed on every year of the study period with available NAIP imagery.

2.3. Model Input Development

The proposed irrigation methods mapping tool uses input imagery constructed from Tier 1 Surface Reflectance data of Landsat missions 5 and 8. Landsat missions provide the longest record of earth observation from space starting with the first Landsat satellite launched in 1972. Landsat missions 5, 7, and 8 were available for the 2003 to 2021 study period but due to the scan line corrector failure of Landsat 7 in 2003, products from this mission were excluded from the study. Landsat 5 covered the period of 2003–2011 and Landsat 8 from 2013 to 2021. Visible, near- and short-wave infrared and thermal bands from these two data sets were used. For Landsat 5, these bands were Bands 1 to 3 for the blue, green and red bands respectively, Bands 4, 5, and 7 for near-infrared, short-wave infrared 1 and short-wave infrared 2 and Band 6 for the thermal band. For Landsat 8, the corresponding bands were Bands 2 to 7 for the visible and infrared bands and Band 10 for the thermal band. Landsat 5 and 8 satellites have a repeat cycle of 16 days which provided the opportunity to capture spatial and temporal patterns associated with different irrigation methods. The proposed approach is based on the assumption that spatial and temporal variations in surface reflectance data provide useful information to differentiate between irrigation

10.1029/2023WR036155

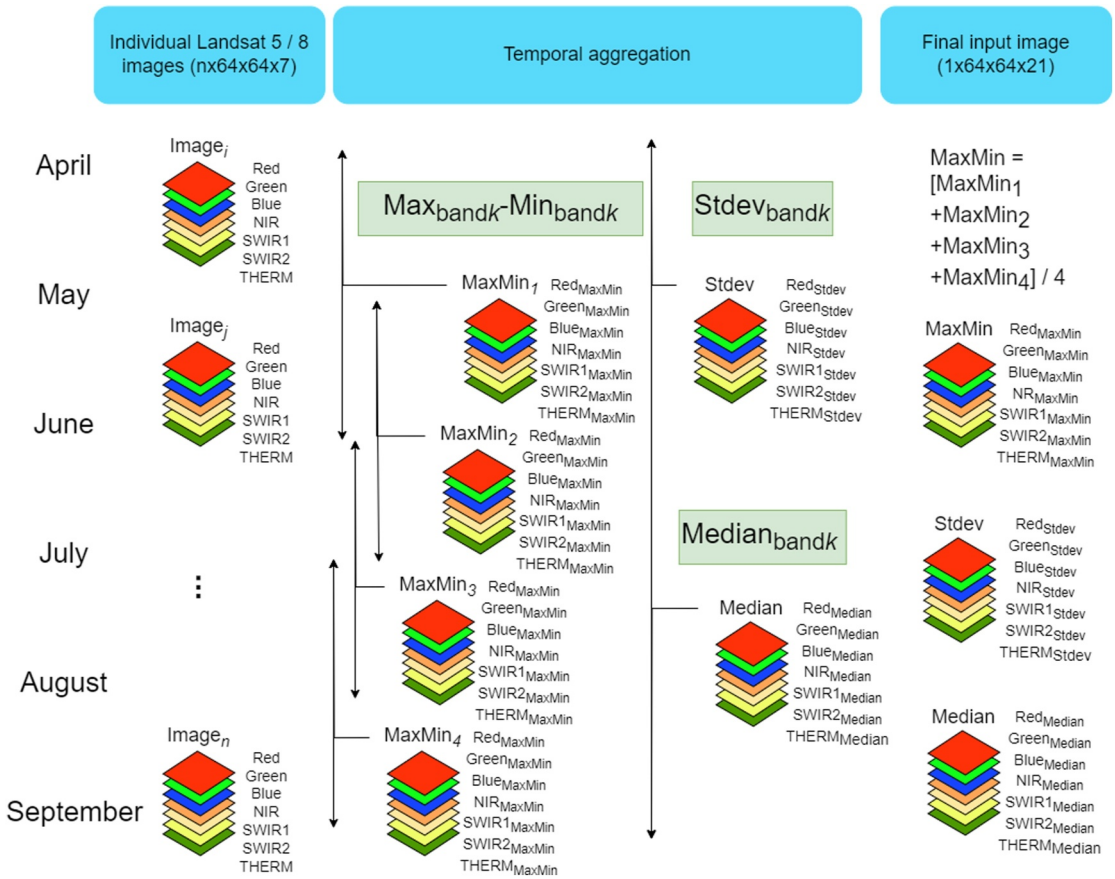

Figure 2. Summary of the input development approach for one sample illustrating Maxima-Minima ($Max_{band} - Min_{band}$), standard deviations (Stdev) and median operations for each of the 7 Landsat bands (Red, Green, Blue, Near Infrared—NIR, Short wave infrared 1 and 2—SWIR1 and SWIR2, and Thermal band—THERM) selected.

methods. To capture temporal patterns in reflectance, model inputs were computed over four 2-month aggregation periods and one 4-month period. These periods were April 1–June 1, May 1–July 1, June 1–August 1, July 1–September 1, and April 1–September 1, abbreviated throughout this paper using only the months (Figure 2). These months correspond to the period when irrigation is the most active in the region. During each of the 2-month aggregation periods, differences between minimum and maximum (max-min) values for each of the Landsat input bands were computed while standard deviations and medians were computed for the April–September period (Figure 2). The four 2-month max-min layers for each band were further averaged to give one average max-min layer per band (Figure 2). Each model input image was therefore made of 21 different channels corresponding to the 7 average max-min values, the 7 median and the 7 standard deviations over the 4-month period. Figure 3 shows an example of input images computed for 5 contiguous field irrigated with different irrigation methods. Circular patterns can be identified in the center pivot (Sprinkler) field while linear wetting features tended to appear where wheel line sprinklers have been utilized. The furrow-irrigated fields (Flood) showed less defined wetting patterns. Each layer in each image was standardized by subtracting cell values by the average of the layer and dividing by the standard deviation. The Google EarthEngine platform (Gorelick et al., 2017) was used to acquire Landsat imagery and compute model inputs. Input images were clipped to 64×64 pixel squares covering the WRLU footprint at a 30 m resolution. The 64×64 pixel squares were spatially independent in the training and evaluation images that is, contiguous squares did not overlap. Input images used at inference were however computed with an overlap of 32 pixels between adjacent squares to reduce edge effects. Between 2003 and 2017, the yearly WRLU survey extent covered a fraction of the entire agricultural area footprint of the State of Utah while the WRLU maps after 2018 covered the entire state. For each square, years with valid WRLU irrigation method information provided sample images for model training and validation. To maintain a balanced data set across years, a maximum of 2000 of the input image squares were extracted each

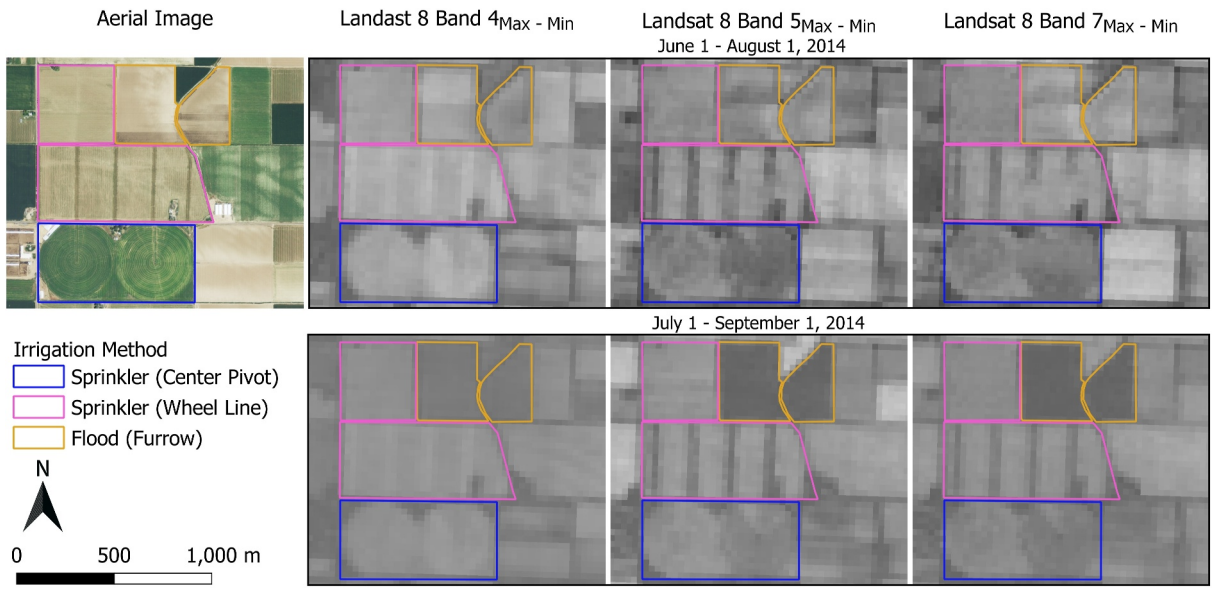

Figure 3. Example of input image layers illustrating spatial patterns associated with wetting patterns of different irrigation methods. Maxima-Minima image layers from Landsat 8 bands 4, 5, and 7 for aggregation periods between June 1 and 1 August 2014 and between July 1 and 1 September 2014 are displayed.

year. Furthermore, to ensure a balance between F, S and O classes in the model, images with greater than 66% O pixels were excluded. Eighty percent of the 64 × 64 squares (training squares) were randomly selected and used for extracting training images while the remaining 20% (validation squares) contributed to validation images. Training squares were spatially distinct from validation squares so that spatial patterns in the training images are not repeated in the validation data set. In total 8,533 training and 2,149 validation images were extracted.

2.4. Proposed FCNN Model

A U-Net architecture was used for the CNN developed for this irrigation mapping approach. The U-Net architecture was developed by Ronneberger et al. (2015) for biomedical imaging. The architecture is composed of a contracting CNN path which captures context in the input images and a symmetric expanding path that allows precise localization of predicted labels. The U-Net architecture has rapidly gained popularity as a classification approach for remotely sensed images (Colligan et al., 2022; Flood et al., 2019; Z. Zhang et al., 2018). As a FCNN, one key advantage of the U-Net architecture is a fast computation time at inference compared to pixel-based methods (Long et al., 2015).

A schematic of the proposed architecture (Figure 4) is similar to that used by Colligan et al. (2022) to map irrigation areas in Montana. The contracting path of the U-Net network consists in a series of the following sequence followed by max pooling layers: 2d convolution layer followed by rectified linear unit (ReLu) activation and batch normalization. Furthermore a dropout layer followed each ReLu activation layer to reduce overfitting and improve generalization (Hinton et al., 2012). A range of dropout rate were tested between 0.01 and 0.2 in 0.01 increment with the value 0.05 yielding satisfactory results in this study. In the expanding path of the U-Net network, we replaced the 2d up-sampling layers used by Colligan et al. (2022) with transposed convolution as used in the original Ronneberger et al. (2015) U-Net implementation. A categorical cross-entropy loss function and the Adam optimizer (Kingma & Ba, 2014) were used to train the U-Net model.

2.5. Data Augmentation and Model Training

To increase the training sample size and improve generalization capability of the ML model, input augmentation was performed on the original images. The augmentation process consisted in a geometric augmentation followed by a radiometric augmentation (Figure 5). The geometric augmentation applied a sequence of random zoom (−30%–30%) followed by a random rotation (-0.8π and 0.8π) and a random bidirectional translation (−20%–20% of the image size) to each original image. Geometric augmentation was applied to each original image four times, thus expanding the training and validation pools to 34,132 and 8,596 images respectively. Geometric

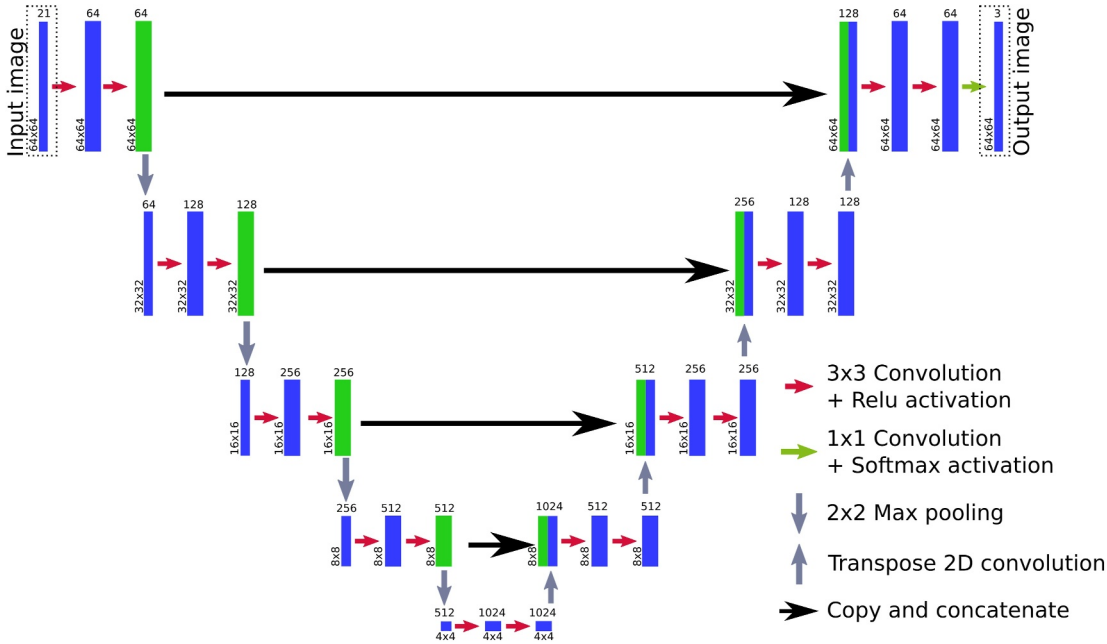

Figure 4. U-Net model architecture developed to map irrigation methods. Inputs are 64 × 64 pixel 21-channel images constructed from Landsat 5 and 8 surface reflectance data. Each blue box represents a multi-channel feature map. Green boxes represent feature maps that are copied and used at subsequent levels of the U-Net network. Image and feature map sizes are indicated at the lower left edge and the number of channels on top of the boxes. The output of the model is a 3-channel image representing Flood/Surface, Sprinkler and Other irrigation methods.

transformation was applied simultaneously to both input and response (irrigation methods) images. The radiometric augmentation consisted in applying a Gaussian noise of random mean −0.0002 to 0.0002 and a standard deviation of 0.002 to each channel of the input image. The radiometric augmentation was applied to the input images at each training iteration. The model was trained using a batch size of 64 and 51 steps per epoch. At each epoch, each of the 16 years with available irrigation methods data contributed 200 randomly selected images,

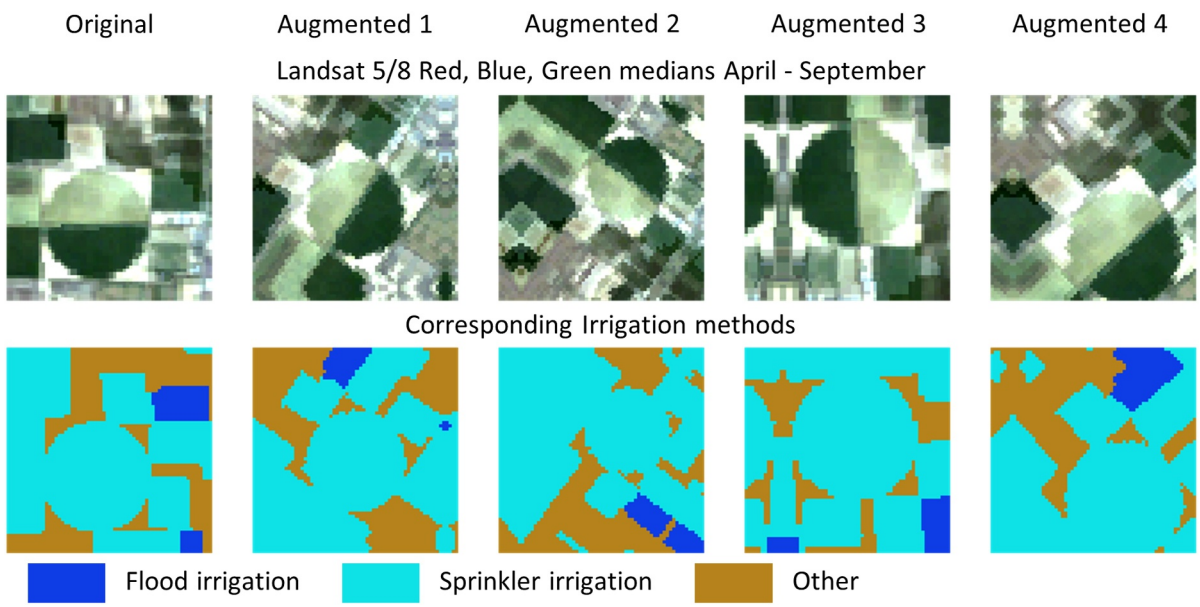

Figure 5. Illustration of the image augmentation process showing the original image which was transformed into a series of augmented images by applying a random zoom (±30%), a random rotation (±0.8π), a random bidirectional translation (−20%–20% of image size). A Gaussian noise of standard deviation 0.002 and random mean (±0.0002) was added to each channel of the geometrically transformed images. Edge pixels were reflected and a nearest neighbor interpolation was used.

resulting in a total of 3,200 images per epoch. This allowed to have a balanced input data set across years. The model was trained using the Tensorflow library (Abadi et al., 2016) on the USDA SCINET Ceres high performance computer using a TESLA V100 GPU. Training was stopped when the loss function on the evaluation data set has stopped decreasing for 50 epochs. To improve performance, 10 separate models were trained, and an ensemble model developed by averaging the outputs of these models.

2.6. Model Performance Evaluation

Model performance was evaluated by building the confusion matrix and calculating the overall accuracy (A) and precision (P), recall (R) and F1 score for each irrigation class from the pixel-to-pixel correspondence between observed and predicted irrigation methods on the evaluation data set. The accuracy expresses the fraction of overall pixels correctly classified by the model. For each class, the precision expresses the fraction of all predicted pixels in the class that are true predictions. The recall is the fraction of all observed pixels of a given class that have been correctly predicted by the model. The F1 score is a measure that balances P and R. The following formula were used to calculate A, P, R, and F1:

$$A = \frac{\sum_{i=F,S,O} TPi}{\sum_{i=F,S,O} TPi + \sum_{i=F,S,O} FNi} \quad (1)$$

$$Pi = \frac{TPi}{TPi + FPi} \quad (2)$$

$$Ri = \frac{TPi}{TPi + FNi} \quad (3)$$

$$F1i = \frac{2 \times Ri \times Pi}{Ri + Pi} \quad (4)$$

where TPi, FPi, FNi are respectively the numbers of true positive, false positives and false negative for irrigation method i. Metrics A, P, R and F1 were calculated for the entire validation set to evaluate the overall performance of the trained model. The performance metrics were also calculated for each year of available validation data to evaluate the temporal stability of the A, P, R and F1 metrics. A third evaluation was performed by calculating performance metrics within five spatially distinct regions to check the spatial stability of the trained model. Four of these regions were quadrangles selected across the WRLU footprint. These regions were Elwood (577 Km^2), Logan (310 Km^2), Richmond (260 Km^2) and Sutherland (525 Km^2), named after the largest town they encompass. The fifth region covered the TFCC footprint, but evaluations were only made within the 1.9 Km squares in which labeled irrigation methods were available.

2.7. Application to TFCC

The trained model was tested on the TFCC area (Figure 1b) to evaluate its effectiveness at predicting irrigation methods outside the WRLU footprint and to evaluate changes in irrigation methods between 2003 and 2021. To reduce year-to-year variability, the predicted irrigation method at a pixel location for a given year was compared to the prediction of the preceding and the following year. The mode of predicted irrigation method at each pixel for these three consecutive years was then chosen. Irrigation methods predictions for years 2006, 2011, 2013, and 2016 were compared to surveys conducted by Bjorneberg et al. (2020). Note that Landsat imagery for 2012 was not available so the 2011 map used years 2010, 2011, and 2013 to compute the mode while the 2013 map used the 2011, 2013, and 2014 predictions.

3. Results and Discussions

3.1. Overall Performance

The 10 trained U-Net models used to develop the ensemble converged after 148 to 212 epochs. Each of the 51 training steps was completed in 290 msec on the TESLA V100 GPU, resulting in training times ranging from 36 to 52 min for the ten U-Net models. The performance of the ensemble model is summarized in Tables 1 and 2. Of

Table 1
Confusion Matrix of the Irrigation Methods Prediction Obtained by Applying the Ensemble of Trained U-Net Models to the Evaluation Data Set

		Predicted pixels			
		Surface/flood	Sprinkler	Other	Total
Observed pixels	Surface/Flood	778225	110688	152051	104096
	Sprinkler	159030	773410	106270	1038710
	Other	132212	58829	1006085	1197126
	Total	1069467	942927	1264406	3276800

Note. Evaluation images were 64 pixels by 64 pixels and comparison with observed data was done on the pixel basis.

the 3,276,800 pixels making up the evaluation data set, 2,557,720 pixels (778225 F, 773410 S and 1,006,085 O pixels) were correctly predicted, resulting in an overall accuracy of 0.78. Precisions achieved by the ensemble model were 0.73, 0.82, and 0.80 for F, S, and O pixel classes respectively (Table 2). The confusion matrix (Table 1) shows that most of the false positives in class F were pixels of class S (159030). Conversely, most false positives in class S were pixels of class F (110688). False positives in class O were more likely to be of class F (152051). Recalls for the F, S, and O classes were respectively 0.75, 0.74, and 0.84 while F1 scores were 0.74, 0.78, and 0.82. These performance metrics were consistent with results from Raei et al. (2022) who published performance values between 72% and 86% on validation data for their proposed approach to segment irrigation method from high-resolution aerial imagery. The method proposed by Raei et al. (2022) uses a U-Net architecture with a ResNet backbone which differs from the traditional U-Net approach used in this study. The U-Net on ResNet backbone approach used by Raei et al. (2022) is often used to deal with the "vanishing gradient" problem which can adversely impact training performance in a gradient-based learning model (Glorot & Bengio, 2010). In our proposed approach, performance achieved were consistent with that tested by Raei et al. (2022), possibly the result of the greater number of input layers which were intended to capture dynamic patterns associated with irrigation methods. It is also important to note that our approach covers a wide geographical area (Utah and southern Idaho) while the Raei et al. (2022) approach was developed and evaluated in 2 counties of southern Idaho. Furthermore, the proposed approach in this paper relies on Landsat satellite products which are widely available across the globe at much higher temporal frequency (16 days) than high resolution aerial imagery which are often unavailable in many parts of the globe and only every two years in the USA through the NAIP program. As a result, the proposed approach in this paper is useful to map yearly changes in irrigation methods and testable in other irrigated regions of the world.

3.2. Performance by Year

Figure 6 shows the results of the evaluation of the ensemble model for each year of available validation data. None of the performance metrics displayed any systematic trend or shift with year, suggesting that the source of Landsat imagery used (Landsat 5 vs. Landsat 8) did not have a measurable impact on model performance. The overall accuracy of the model ranged from 0.70 to 0.91 with an average of 0.77. Precision values ranged from 0.55 to 0.93 with an average of 0.77 while R ranged 0.53–0.94 with an average of 0.76. F1 scores ranged 0.58–0.93 with an average of 0.76. The model tended to have the lowest performance for flood irrigation prediction especially based on the precision and F1 score.

3.3. Performance in Test Regions

Results of the performance evaluation by region are summarized in Table 3. Figure 7 shows observed versus predicted maps for two example years in each region. Accuracy values in most test regions were consistent with the 0.78 overall accuracy of the model (Table 2). Accuracy was the highest in the Elwood region (0.79) and lowest in the Logan (0.59) and Richmond (0.59) regions. Figure 7 shows that many of the S irrigated areas in the Logan and Richmond quadrangles were incorrectly predicted as F. Many of the mismatches occur in areas where small areas of one irrigation class appear within large blocks of another class, suggesting that the U-Net models were not highly sensitive to small individual fields but relied on broad spatial patterns to accurately recognize irrigation methods. Accuracy values estimated from these maps were 0.82, 0.64, 0.66 and 0.78 for Elwood, Logan, Richmond and Sutherland respectively thus, in agreement with those reported in Table 3. This suggests that the 32-pixel overlap between contiguous squares used at inference did not adversely affect performance. The coarse resolution of the Landsat bands (30 m for RGB and SWIR and 60 m for the thermal band) likely limits the ability of small spatial features to be accurately capture by the U-Net models. Improvements may be possible with the use of higher resolution satellite products such as Sentinel 2. The Sutherland region was dominated by flood

Table 2
Results of the Evaluation of the Ensemble of Trained U-Net Models Showing Overall Accuracy (A), Precision (P), Recall (R) and F1-Score (F1) Calculated From Pixel-To-Pixel Comparisons Between Predicted and Observed Irrigation Methods

	Precision (P)	Recall (R)	F1-score (F1)	Accuracy (A)
Surface/flood	0.73	0.75	0.74	
Sprinkler	0.82	0.74	0.78	0.78
Other	0.80	0.84	0.82	

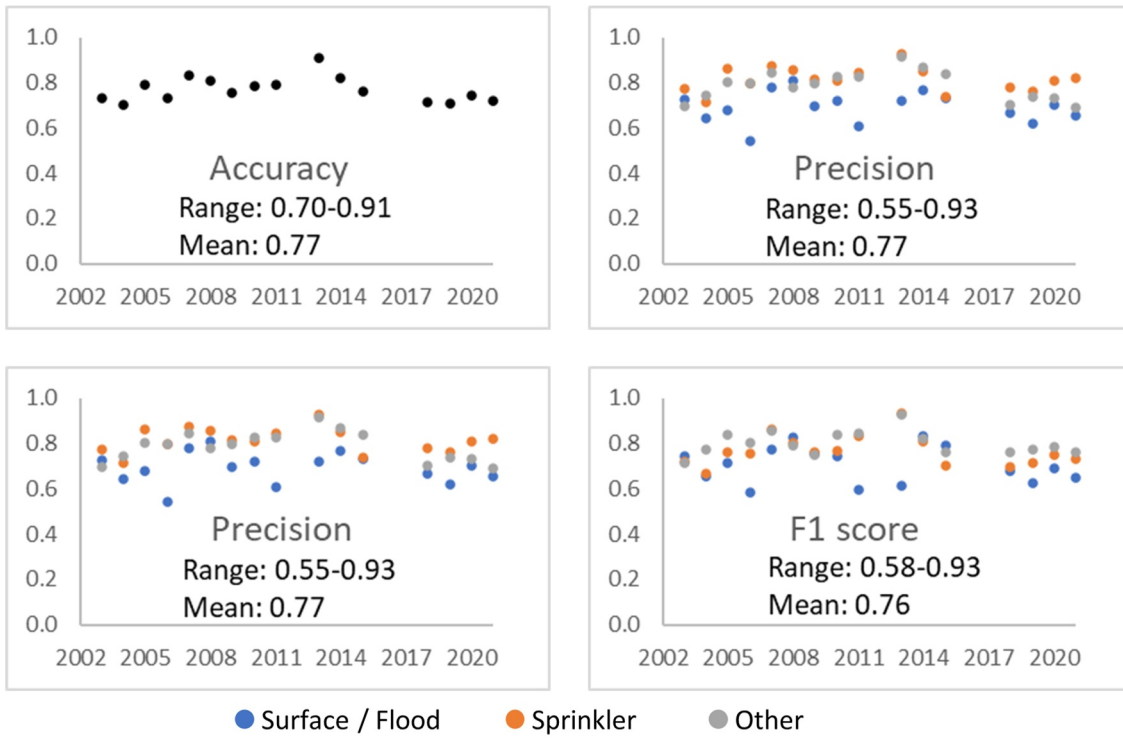

Figure 6. Accuracy, precision, recall and F1 score obtained by evaluating the trained U-Net model for each year with available validation data.

irrigation which was adequately predicted ($P = 0.91$ and $R = 0.77$) by the trained model. The model performed well in the TFCC area (Figure 7) with an accuracy of 0.70 which was slightly less than the 0.78 overall accuracy but greater than the accuracy achieved in the Logan and Richmond regions of the WRLU footprint. Despite the comparatively small proportion of the training data that was collected in the TFCC irrigation project, the model performed well at predicting S irrigation in TFCC ($P = 0.72$, $R = 0.85$, and $F1 = 0.78$) but greater confusion was observed between F and O classes ($F1 = 0.57$ and 0.63 for F and O respectively). It is important to note that the WRLU data set encompasses some irrigation methods under the O category (e.g., sub-irrigated and dryland farming) that are not common in the TFCC region. Furthermore, surface irrigation practices are constrained by topography, water delivery infrastructure, and other local factors which may have resulted in slightly different spatio-temporal patterns in TFCC compared to areas in the WRLU footprint. Nevertheless, in TFCC most irrigated areas are either F or S with negligible occurrences of other irrigation methods. Most of the O prediction in this region can therefore be reclassified as F.

Table 3
Results of the Evaluation of the Ensemble of Trained U-Net Models in Test Areas Near the Utah Towns of Elwood, Logan, Richmond, Sutherland and in the Twin Falls Canal Company Irrigation Project in Southern Idaho

		Precision			Recall			F1		
	Accuracy	F	S	O	F	S	O	F	S	O
Elwood	0.79	0.84	0.49	0.76	0.92	0.53	0.50	0.88	0.51	0.60
Logan	0.59	0.61	0.48	0.65	0.83	0.39	0.41	0.71	0.43	0.50
Richmond	0.59	0.20	0.85	0.73	0.63	0.60	0.55	0.30	0.70	0.63
Sutherland	0.74	0.91	0.1	0.46	0.77	0.69	0.58	0.83	0.17	0.51
TFCC	0.70	0.60	0.72	0.83	0.54	0.85	0.51	0.57	0.78	0.63

Note. Performance metrics are overall accuracy (A), precision (P), recall (R) and F1-score (F1) calculated from pixel-to-pixel comparisons between predicted and observed irrigation methods. P, R and F1 are reported for each irrigation class labeled as F for Surface/Flood irrigation, S for sprinkler irrigation and O for Other.

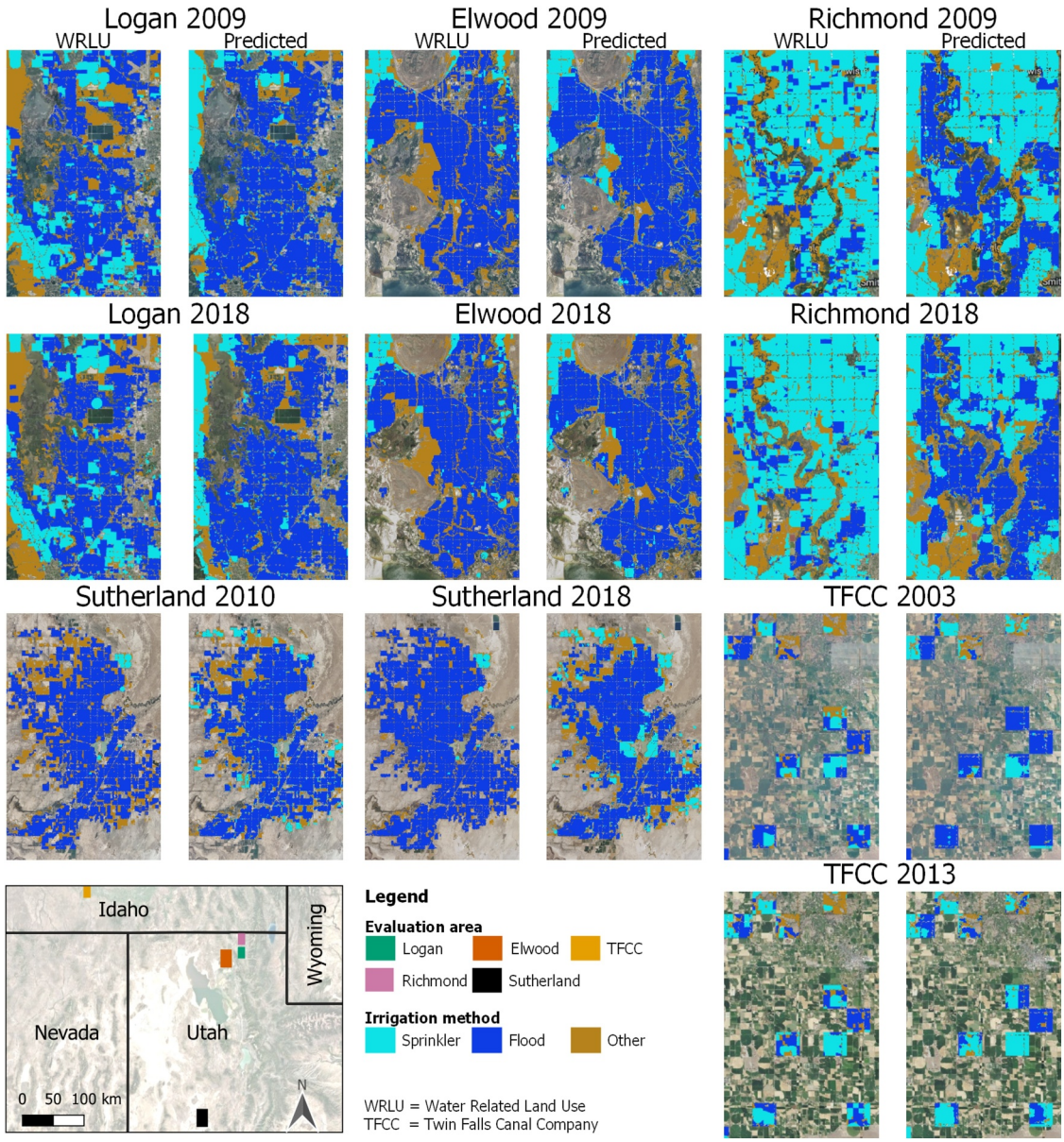

Figure 7. Maps of observed irrigation methods from the Water Related Land Use (WRLU) data set compared with predictions made using the ensemble of trained U-Net models for years 2009 (a) and 2018 (b) in test areas across the WRLU spatial footprint. U-Net model input images were developed from Landsat 5 for year 2009 and Landsat 8 for year 2018.

3.4. Application to TFCC and Implication for Irrigation Water Management

Figure 8 shows the maps of irrigation methods predicted for the TFCC irrigation project for years 2006, 2010 and 2013. These maps confirm the progressive conversion of surface irrigation to sprinkler systems. In 2006, 41.1% of the agricultural land was classified as F whereas 51.9% was classified as S. In 2011, the F pixels decreased to 35.2% while the S pixels increased to 56.7%. Further conversion was observed by 2016 when F made up only 30.5% of classified pixels while S pixels increased to 61.1%. The proportion of O pixels remained stable between 2006 and 2016, ranging only between 7.0% and 8.4%.

Using surveys conducted on aerial imagery, Bjorneberg et al. (2020) found that sprinkler irrigation was 46%, 52%, 54%, and 59% of surveyed areas in 2006, 2011, 2013, and 2016 respectively (Figure 9). These results were slightly lower but mostly within 5% of the 51.9%, 56.7%, 61.7%, and 61.1% values obtained using the ensemble model. Besides the inherent accuracy limit of the ensemble model, additional factors controlling the gap between the

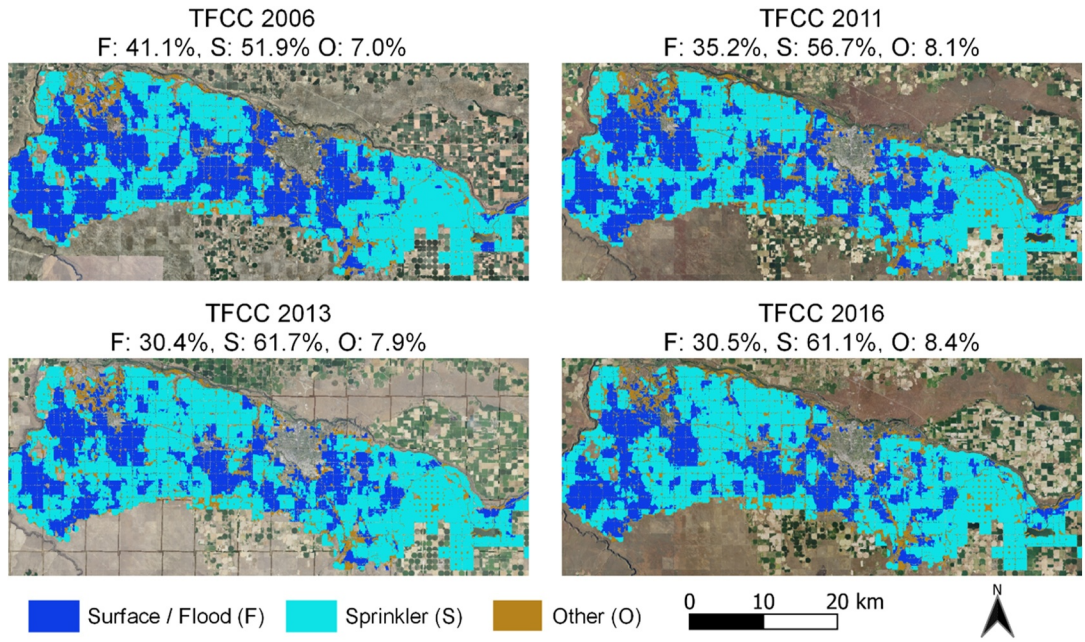

Figure 8. Irrigation methods prediction in the Twin Falls Canal Company irrigation project for years 2006, 2011, 2013, and 2016. The percentage of agricultural areas irrigated with each irrigation method was calculated from the prediction maps.

Bjorneberg et al. (2020) findings and our results include the use of the 3-year mode to map irrigation methods, and the smaller survey area (3,500 ha or 4% of the TFCC land area) used in the Bjorneberg et al. (2020) study. In particular, the use of the 3-year mode in the development of the irrigation methods maps introduced a positive bias for sprinkler irrigation prediction since this irrigation method was increasingly adopted in TFCC during the study period. Overall, the conversion rate to sprinklers in TFCC was estimated to be 1.4% per year using the ensemble model (Figure 9). This conversion rate is consistent with the 1.5% rate noted in Bjorneberg et al. (2020). Nevertheless, Figure 9 also shows some temporary decline in the rate of conversion, particularly from 2014 to 2017 and after 2019. These decreases in conversion rate are the result of prediction errors in the U-Net model since retrograde conversion from sprinkler to flood or furrow irrigation is highly uncommon. The marked decrease in conversion rate predicted by the U-Net model during the 2014–2017 period was driven by a very poor performance of the model in 2016, suggesting that the absence of 2016 WRLU training data degraded prediction quality for this year.

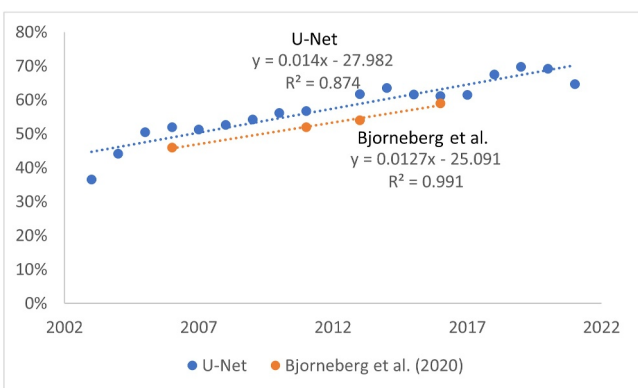

Figure 9. Estimated proportion of agricultural land irrigated with sprinkler irrigation in the Twin Falls Canal company irrigation project using the ensemble of trained U-Net models compared to the Bjorneberg et al. (2020) survey.

Figure 9 demonstrates the ability of the trained ensemble model to map irrigation methods for past and present conditions. As noted above, the irrigation methods predictions reveal the dominant irrigation in an area as small fields of contrasting irrigation class than their surroundings are not well resolved. The TFCC irrigation methods maps show that conversion to sprinkler across the irrigation project seem to occur in spatial clusters that expand over time. Much of the eastern part of the TFCC irrigation project was dominated by sprinkler systems by the early 1990s. From the mid-1990s, many fields have been converted to sprinkler irrigation with financial assistance from the Environmental Quality Incentive Program and other special projects. In converting to sprinkler systems, center pivot systems are highly desirable due to their low labor requirement but their expansion into new areas can be constrained by the access to high voltage electricity. Figure 9 shows that sprinkler irrigation makes up nearly 70% of the agricultural land in the TFCC project in the most recent estimates. Areas in future need of conversion to sprinklers can be identified using maps shown in Figure 8. This type of information will be valuable for resource management agency for identifying and targeting priority areas. Furthermore, in many regions of the

world, investments are being made in irrigation technology to improve outcomes on water quantity and quality (Perry et al., 2017). Many of these investments include the conversion from surface irrigation to sprinkler systems. Perry et al. (2017) noted that understanding the effects of improvements in irrigation technology on water resources requires a nuanced consideration of multiple factors as improvements in technology does not automatically translate into water savings. The ability to map areas where conversion from surface to sprinkler irrigation has occurred would provide much needed insights into the impact of sprinkler conversion on local and regional water resources.

The ability of the proposed irrigation mapping approach to be applied to other irrigated watersheds depends on many factors including the level of aridity of the target area and the method of irrigation to be mapped. The input data used to train the UNet models originate from semi-arid regions where natural precipitation amounts during the growing season are very low. Most of the productive agricultural farms are therefore significantly irrigated, leading to distinct contrasts between irrigated areas and non-irrigated areas. As a result, the approach developed in this paper might not be suitable in regions where natural precipitation amounts can support crop growth. The predominant irrigation methods mapped by the proposed are center pivot and wheel line irrigation under sprinkler systems and flood irrigation. The UNet models were therefore trained to recognize spatio-temporal patterns associated with these three irrigation types. Other sprinkler irrigation types such as linear move, solid sets or micro-irrigation systems were not abundantly represented in the training data. The developed approach is therefore limited to regions characterized by low precipitation amount during the growing season and where the main irrigation methods used are center pivot, wheel line and flood irrigation. The northwestern U.S. encompasses many such agricultural regions. Agricultural basins in eastern Washington, eastern Oregon, northern California, Nevada, Utah, Montana, Colorado and Wyoming are examples of regions where the proposed approach could be tested. Other regions of the world where the proposed approach can be tested include the Middle East and North Africa region where natural precipitation for crop growth is low and surface irrigation accounts for 86.6% of the irrigation methods versus 8.7% for sprinkler irrigation (Frenken, 2009).

Irrigation methods are rapidly changing in many irrigated regions of the world, including in the western USA. Traditional surface irrigation methods such as flood irrigation are being upgraded to sprinkler systems, generally leading to improvements in irrigation efficiency at the field scale (Al-Jamal et al., 2001; Bjorneberg et al., 2020). These field-scale improvements do not always result in water savings at the watershed scale because some irrigation projects supply irrigation water based on water availability rather than crop water demand (Bjorneberg et al., 2020) while others show reductions in water volumes diverted for irrigation post-conversion (Sando et al., 1988). Conversion from surface irrigation to sprinkler systems is often associated with water quality improvements at the watershed scale (Bjorneberg et al., 2020; Nouwakpo et al., 2023) owing to the improved infiltration and reduced runoff under sprinkler systems. Understanding the relationship between changes in irrigation methods and irrigation efficiency at the basin scale requires a nuanced approach that takes into account information on the location of various irrigation methods across the landscape. Mapping irrigation methods at broad spatial scale is therefore needed to better assess impact on water resources. The mapping technique developed in this paper offers the advantage of being testable in other irrigated regions of the world, many of which play a crucial role on global food security. In many parts of the world, increasing population and a changing climate create an increasing need for more accurate accounting of freshwater use, particularly for irrigation, the largest share of freshwater withdrawals. In the USA, the U.S. Geological Survey produces estimates of water use for various water use categories every 5 years since 1950 as part of the SECURE Water Act (Public Law 111–11, 123 Stat. 991) (Painter et al., 2021). These estimates classify irrigation water use by the type of irrigation method using survey data. These survey data provide aggregated information on the proportion of irrigation methods in a geographical area (state, county, etc.) but do not inform on the spatial distribution of irrigation methods. The technique proposed in this paper has the potential to routinely track the spatial distribution of irrigation methods on the landscape in addition to providing timely aggregates of state- and county-level information on irrigation methods. Irrigation method maps such as those created in this paper can also improve hydrologic modeling of surface and groundwater resources in irrigated watersheds where the influence of a given irrigation method depends as much on its abundance in the watershed as its relative position along drainage networks.

4. Conclusions

In this paper, we developed a deep learning approach to map irrigation methods in agricultural regions where surface irrigation and sprinkler systems are dominant. The U-Net architecture employed for this modeling

technique adequately mapped irrigation methods with an overall accuracy of 0.78. Performance of the model was temporally stable but varied in space. The trained U-Net models were used to develop maps of irrigation methods for an irrigated watershed in Southern Idaho. Comparison of sprinkler irrigation estimates from these predicted maps were in alignment with previously published data. The ability to accurately capture field-level details was limited by the coarse resolution of the Landsat images used as model input. This new tool will help water management stakeholders in their efforts to improve water availability and quality in irrigated areas. The developed maps are suitable for assessing changes in irrigation practices at broad spatial scales and useful to identify priority areas in need of future conversion from surface irrigation to sprinkler irrigation. The proposed approach has potential application in other irrigated areas where rainfall input during the growing season is minimal and irrigation methods are varied across the landscape. Nevertheless, because this approach was developed using data predominantly from Utah, it is unclear if achieved performance will be maintained in other irrigated regions of the western USA and the world. There is a need for further evaluation of the proposed approach in other irrigated regions where irrigation methods maps are available for transfer learning and performance evaluation. The 30-m resolution of the Landsat imagery may also be a limiting factor in areas where agricultural fields are small in size. Furthermore, as a machine learning method, the U-Net approach developed in this paper does not inform on the specific biophysical and/or interferometric processes aiding in the segmentation between irrigation method classes. It is therefore unclear how this technique will perform in areas with drastically different crops and water availability constraints than those prevailing in Utah and Southern Idaho. In this study, Landsat images were temporally aggregated into input images for the U-Net model. The choice of this temporal aggregation method required some trial and error but could be obviated in future work with the integration of suitable deep learning approach for sequential data such as Recurrent Neural Networks.

Data Availability Statement

The WRLU data set is available at https://gis.utah.gov/data/planning/water-related-land. Additionally labeled irrigation methods of agricultural fields in southern Idaho and input/output processing and model training codes are available for download at https://datadryad.org/stash/share/gaPC9SliGpvUVUCfNlgZxdcpRQ2DDadOKT-OA9Dovh4. Codes are also are available at https://github.com/oishee-hoque/Land-Segmentation-Based-on-Irrigation-Type.

Acknowledgments
The authors would like to thank Mr. Xander Laraway, Mr. Carlos Kelly, and Mr. Jared Knott for their help digitizing and labeling agricultural fields of southern Idaho.

References

Abadi, M., Agarwal, A., Barham, P., Brevdo, E., Chen, Z., Citro, C., et al. (2016). Tensorflow: Large-scale machine learning on heterogeneous distributed systems. arXiv preprint arXiv:1603.04467.

Al-Jamal, M., Ball, S., & Sammis, T. (2001). Comparison of sprinkler, trickle and furrow irrigation efficiencies for onion production. *Agricultural Water Management*, *46*(3), 253–266. https://doi.org/10.1016/S0378-3774(00)00089-5

Bazzi, H., Baghdadi, N., Ienco, D., El Hajj, M., Zribi, M., Belhouchette, H., et al. (2019). Mapping irrigated areas using sentinel-1 time series in Catalonia, Spain. *Remote Sensing*, *11*(15), 25. https://doi.org/10.3390/rs11151836

Bjorneberg, D., King, B., & Koehn, A. (2020). Watershed water balance changes as furrow irrigation is converted to sprinkler irrigation in an arid region. *Journal of Soil and Water Conservation*, *75*(3), 254–262. https://doi.org/10.2489/jswc.75.3.254

Boken, V. K., Hoogenboom, G., Kogan, F. N., Hook, J. E., Thomas, D. L., & Harrison, K. A. (2004). Potential of using NOAA-AVHRR data for estimating irrigated area to help solve an inter-state water dispute. *International Journal of Remote Sensing*, *25*(12), 2277–2286. https://doi.org/10.1080/01431160310001618077

Brouwer, C., Prins, K., Kay, M., & Heibloem, M. (1988). Irrigation water management: Irrigation methods. *Training manual*, *9*(5), 5–7.

Chauhan, R., Ghanshala, K. K., & Joshi, R. C. (2018). Convolutional neural network (CNN) for image detection and recognition. In *2018 first international conference on secure cyber computing and communication (ICSCCC)* (pp. 278–282). https://doi.org/10.1109/ICSCCC.2018.8703316

Colligan, T., Ketchum, D., Brinkerhoff, D., & Maneta, M. (2022). A deep learning approach to mapping irrigation using landsat: Irrmapper U-Net. *IEEE Transactions on Geoscience and Remote Sensing*, *60*, 1–11. https://doi.org/10.1109/tgrs.2022.3175635

de Albuquerque, A. O., de Carvalho Júnior, O. A., Carvalho, O. L. F. d., de Bem, P. P., Ferreira, P. H. G., de Moura, R. d. S., et al. (2020). Deep semantic segmentation of center pivot irrigation systems from remotely sensed data. *Remote Sensing*, *12*(13), 2159. https://doi.org/10.3390/rs12132159

Dieter, C. A., Maupin, M., Caldwell, R., Harris, M., Ivahnenko, T., Lovelace, J., et al. (2018). *Estimated use of water in the United States in 2015: U.S. Geological survey circular 1441*. (Report No. 141134233X). U.S. Geological Survey. https://doi.org/10.3133/cir1441

Eckhoff, J., & Bergman, J. (2001). Sugarbeet (beta vulgaris) production under sprinkler and flood irrigation. In *Proceedings from the 31st biennial meeting (agriculture) of the american society of sugar beet technologists, Vancouver, BC, Canada* (pp. 239–241). 28 February–3 March, 2001.

Farahani, S. S., Asoodar, M. A., & Moghadam, B. K. (2020). Short-term impacts of biochar, tillage practices, and irrigation systems on nitrate and phosphorus concentrations in subsurface drainage water. *Environmental Science and Pollution Research*, *27*(1), 761–771. https://doi.org/10.1007/s11356-019-06942-w

Flood, N., Watson, F., & Collett, L. (2019). Using a U-net convolutional neural network to map woody vegetation extent from high resolution satellite imagery across Queensland, Australia. *International Journal of Applied Earth Observation and Geoinformation*, *82*, 101897. https://doi.org/10.1016/j.jag.2019.101897

Food and Agriculture Organization of the United Nations (FAO). (2018). AQUASTAT - FAO's global information system on water and agriculture. Retrieved from https://www.fao.org/aquastat/en/

Franco-Luesma, S., Cavero, J., Plaza-Bonilla, D., Cantero-Martínez, C., Tortosa, G., Bedmar, E. J., & Álvaro Fuentes, J. (2020). Irrigation and tillage effects on soil nitrous oxide emissions in maize monoculture. *Agronomy Journal*, *112*(1), 56–71. https://doi.org/10.1002/agj2.20057

Frenken, K. (2009). Irrigation in the middle east region in figures aquastat survey-2008.

Fukushima, K. (1979). Neural network model for a mechanism of pattern recognition unaffected by shift in position-neocognitron. *IEICE Technical Report, A*, *62*(10), 658–665.

Glorot, X., & Bengio, Y. (2010). Understanding the difficulty of training deep feedforward neural networks. In *Proceedings of the thirteenth international conference on artificial intelligence and statistics* (pp. 249–256).

Gorelick, N., Hancher, M., Dixon, M., Ilyushchenko, S., Thau, D., & Moore, R. (2017). Google Earth Engine: Planetary-scale geospatial analysis for everyone. *Remote Sensing of Environment*, *202*, 18–27. https://doi.org/10.1016/j.rse.2017.06.031

Hinton, G. E., Srivastava, N., Krizhevsky, A., Sutskever, I., & Salakhutdinov, R. R. (2012). Improving neural networks by preventing co-adaptation of feature detectors. arXiv preprint arXiv:1207.0580.

Hoeser, T., & Kuenzer, C. (2020). Object detection and image segmentation with deep learning on earth observation data: A review-part i: Evolution and recent trends. *Remote Sensing*, *12*(10), 1667. https://doi.org/10.3390/rs12101667

Huang, B., Lu, K., Audeberr, N., Khalel, A., Tarabalka, Y., Malof, J., et al. (2018). Large-scale semantic classification: Outcome of the first year of inria aerial image labeling benchmark. In *IGARSS 2018-2018 ieee international geoscience and remote sensing symposium* (pp. 6947–6950).

Ippolito, J. A., Bjorneberg, D. L., Blecker, S. W., & Massey, M. S. (2019). Mechanisms responsible for soil phosphorus availability differences between sprinkler and furrow irrigation. *Journal of Environmental Quality*, *48*(5), 1370–1379. https://doi.org/10.2134/jeq2019.01.0016

Kattenborn, T., Leitloff, J., Schiefer, F., & Hinz, S. (2021). Review on convolutional neural networks (CNN) in vegetation remote sensing. *ISPRS Journal of Photogrammetry and Remote Sensing*, *173*, 24–49. https://doi.org/10.1016/j.isprsjprs.2020.12.010

Kingma, D. P., & Ba, J. (2014). Adam: A method for stochastic optimization. arXiv preprint arXiv:1412.6980.

Long, J., Shelhamer, E., & Darrell, T. (2015). Fully convolutional networks for semantic segmentation. In *Proceedings of the IEEE conference on computer vision and pattern recognition* (pp. 3431–3440).

Lv, G., Kang, Y., Li, L., & Wan, S. (2010). Effect of irrigation methods on root development and profile soil water uptake in winter wheat. *Irrigation Science*, *28*(5), 387–398. https://doi.org/10.1007/s00271-009-0200-1

Nachabe, M. H., Ahuja, L. R., & Butters, G. (1999). Bromide transport under sprinkler and flood irrigation for no-till soil condition. *Journal of Hydrology*, *214*(1), 8–17. https://doi.org/10.1016/S0022-1694(98)00222-4

Naghedifar, S. M., Ziaei, A. N., & Ansari, H. (2018). Simulation of irrigation return flow from a Triticale farm under sprinkler and furrow irrigation systems using experimental data: A case study in arid region. *Agricultural Water Management*, *210*, 185–197. https://doi.org/10.1016/j.agwat.2018.07.036

Nouwakpo, S., Bjorneberg, D., & Rogers, C. (2023). Patterns and associations between dominant crop productions and water quality in an irrigated watershed. *Journal of Soil and Water Conservation*, *78*(6), 466–478. https://doi.org/10.2489/jswc.2023.00176

Painter, J. A., Brandt, J. T., Caldwell, R. R., Haynes, J. V., & Read, A. L. (2021). *Documentation of methods and inventory of irrigation information collected for the 2015 US Geological Survey estimated use of water in the United States* (Tech. Rep.). US Geological Survey.

Perry, C., Steduto, P., & Karajeh, F. (2017). *Does improved irrigation technology save water? A review of the evidence* (Vol. 42). Food and Agriculture Organization of the United Nations.

Pervez, M. S., & Brown, J. F. (2010). Mapping irrigated lands at 250-m scale by merging MODIS data and national agricultural statistics. *Remote Sensing*, *2*(10), 2388–2412. https://doi.org/10.3390/rs2102388

Raei, E., Asanjan, A. A., Nikoo, M. R., Sadegh, M., Pourshahabi, S., & Adamowski, J. F. (2022). A deep learning image segmentation model for agricultural irrigation system classification. *Computers and Electronics in Agriculture*, *198*, 106977. https://doi.org/10.1016/j.compag.2022.106977

Rodrigues, M. L., Körting, T. S., & de Queiroz, G. R. (2020). Circular hough transform and balanced random forest to detect center pivots. In *Geoinfo* (pp. 106–117).

Ronneberger, O., Fischer, P., & Brox, T. (2015). U-net: Convolutional networks for biomedical image segmentation. In *Medical image computing and computer-assisted intervention–MICCAI 2015: 18th International Conference, Munich, Germany, October 5-9, 2015, Proceedings, Part III* (Vol. 18, pp. 234–241). https://doi.org/10.1007/978-3-319-24574-4_28

Salmon, J. M., Friedl, M. A., Frolking, S., Wisser, D., & Douglas, E. M. (2015). Global rain-fed, irrigated, and paddy croplands: A new high resolution map derived from remote sensing, crop inventories and climate data. *International Journal of Applied Earth Observation and Geoinformation*, *38*, 321–334. https://doi.org/10.1016/j.jag.2015.01.014

Sando, S. K., Borrelli, J., & Brosz, D. J. (1988). Hydrologic impacts of improved irrigation efficiencies. *Journal of Irrigation and Drainage Engineering*, *114*(2), 334–342. https://doi.org/10.1061/(ASCE)0733-9437(1988)114:2(334

Saraiva, M., Protas, E., Salgado, M., & Souza, C. (2020). Automatic mapping of center pivot irrigation systems from satellite images using deep learning. *Remote Sensing*, *12*(3), 14. https://doi.org/10.3390/rs12030558

Siebert, S., Döll, P., Hoogeveen, J., Faures, J.-M., Frenken, K., & Feick, S. (2005). Development and validation of the global map of irrigation areas. *Hydrology and Earth System Sciences*, *9*(5), 535–547. https://doi.org/10.5194/hess-9-535-2005

Siebert, S., Kummu, M., Porkka, M., Döll, P., Ramankutty, N., & Scanlon, B. R. (2015). A global data set of the extent of irrigated land from 1900 to 2005. *Hydrology and Earth System Sciences*, *19*(3), 1521–1545. https://doi.org/10.5194/hess-19-1521-2015

Tang, J. W., Arvor, D., Corpetti, T., & Tang, P. (2021). Mapping center pivot irrigation systems in the southern Amazon from Sentinel-2 images. *Water*, *13*(3), 17. https://doi.org/10.3390/w13030298

Thenkabail, P. S., Schull, M., & Turral, H. (2005). Ganges and Indus river basin land use/land cover (LULC) and irrigated area mapping using continuous streams of MODIS data. *Remote Sensing of Environment*, *95*(3), 317–341. https://doi.org/10.1016/j.rse.2004.12.018

Trout, T. J., Kincaid, D. C., & Westermann, D. T. (1994). Comparison of Russet Burbank yield and quality under furrow and sprinkler irrigation. *American Potato Journal*, *71*(1), 15–28. https://doi.org/10.1007/BF02848742

UNESCO. (2018). *United Nations world water development report, nature-based solutions for water* (Report). UNESCO World Water Assessment Programme.

USDA-NASS. (2019). *2018 irrigation and water management survey*. United States Department of Agriculture - National Agricultural Statistics Service (USDA-NASS).

USDA-NASS. (2021). *State agriculture overview: Utah*. USDA-National Agricultural Statistics Service. Retrieved from https://www.nass.usda.gov/Quick_Stats/Ag_Overview/stateOverview.php?state=UTAH

USDA-NRCS. (2012). *National engineering handbook, part 623, chapter 4, surface irrigation*. United States Department of Agriculture Natural Resources and Conservation Service, National Technical Information Service.

USDA-NRCS. (2016). *National engineering handbook, part 623, chapter 11, sprinkler irrigation*. United States Department of Agriculture Natural Resources and Conservation Service, National Technical Information Service.

Utah-DNR. (2022). *Water-related land use inventories: Statewide 2021 inventory*. Utah Department of Natural Resources, Division of Water Resources.

Wada, Y., Flörke, M., Hanasaki, N., Eisner, S., Fischer, G., Tramberend, S., et al. (2016). Modeling global water use for the 21st century: The water futures and solutions (WFAS) initiative and its approaches. *Geoscientific Model Development*, *9*(1), 175–222. https://doi.org/10.5194/gmd-9-175-2016

Xie, Y., Gibbs, H. K., & Lark, T. J. (2021). Landsat-based irrigation dataset (LANID): 30 m resolution maps of irrigation distribution, frequency, and change for the US, 1997–2017. *Earth System Science Data*, *13*(12), 5689–5710. https://doi.org/10.5194/essd-13-5689-2021

Zhang, C. X., Yue, P., Di, L. P., & Wu, Z. Y. (2018). Automatic identification of center pivot irrigation systems from landsat images using convolutional neural networks. *Agriculture-Basel*, *8*(10), 19. https://doi.org/10.3390/agriculture8100147

Zhang, Z., Liu, Q., & Wang, Y. (2018). Road extraction by deep residual u-net. *IEEE Geoscience and Remote Sensing Letters*, *15*(5), 749–753. https://doi.org/10.1109/LGRS.2018.2802944